

# Chapter 10

## Non-Born–Oppenheimer Molecular Dynamics for Conical Intersections, Avoided Crossings, and Weak Interactions

Ahren W. Jasper\* and Donald G. Truhlar†

1. Introduction . . . . .	376
2. Non-Born–Oppenheimer Molecular Dynamics . . . . .	379
2.1. Coupled potential energy surfaces . . . . .	379
2.2. Efficient integration of NBO trajectories . . . . .	382
2.3. Initial conditions for photochemistry . . . . .	386
3. Fewest Switches with Time Uncertainty . . . . .	388
4. Coherent Switches with Decay of Mixing . . . . .	396
5. Summary of Recent Tests and Applications . . . . .	401
6. Concluding Remarks . . . . .	409
6. Acknowledgments . . . . .	410
6. Referneces . . . . .	410

---

\*Combustion Research Facility, Sandia National Laboratories, PO Box 969, Livermore, CA 94551-0969, USA.

†Department of Chemistry and Supercomputing Institute, University of Minnesota, 207 Pleasant Street S.E., Minneapolis, MN 55455-0431, USA.

## 1. Introduction

Processes involving nonradiative transitions between electronic states are ubiquitous in chemistry — from spin-forbidden reactions in combustion to light harvesting in solar cells — and they occur via a variety of elementary chemical mechanisms, such as intersystem crossing, internal conversion, and nonadiabatic electron transfer. The term “non-Born–Oppenheimer” (NBO) may be generally applied to these processes to emphasize the idea that the Born–Oppenheimer separation of the nuclear and electronic time scales breaks down and that potential energy surfaces other than the ground-electronic-state adiabatic potential energy surface play a role in the dynamics. A detailed understanding of NBO coupling of adiabatic electronic states and of the potential energy surfaces associated with them and the ability to predict the effect of this kind of coupling for real chemical systems remain significant challenges to current theories.

One may begin to understand NBO dynamics<sup>1–6</sup> in terms of features of the coupled potential energy surfaces, and in the past we have made the distinction between conical intersections (CIs) of adiabatic surfaces, avoided crossings (ACs) of adiabatic surfaces, and weak interactions (WIs)<sup>7,8</sup> of adiabatic electronic states.

The CIs are  $(F - 2)$ -dimensional hyperseams of degenerate pairs of potential energy surfaces<sup>9</sup> where  $F$  is the number of internal nuclear degrees of freedom, which is  $3N - 6$  for general polyatomics, where  $N$  is the number of atoms. (Sometimes more than two surfaces intersect,<sup>3,10</sup> but this paragraph applies to the simplest case of two.) The surfaces form a double cone<sup>4,11</sup> in the two nondegenerate degrees of freedom, and the CI provides an ultrafast decay route from the higher-energy state in the coupled pair to the lower-energy one. The prominent role of conical intersections in promoting such radiationless decay route was first emphasized by Teller<sup>9</sup>; and it was later used for mechanistic explanations of photochemical reactions.<sup>12–16</sup> Until recently, though, the organic photochemical literature usually associated these decay routes with avoided crossings and regions where potential surfaces approach closely but do not actually cross — such regions were called funnels or bifunnels, which are terms now usually applied to CIs.<sup>17,18</sup> However, the older arguments<sup>9,19</sup> that lead to a correct understanding of the dimensionality of avoided crossings also make it clear that the conical intersections are much more common than fully avoided crossings. Furthermore, since the crossings have a high dimensionality, the seam of crossings can extend over a wide range of geometries, and

this can make the dynamics more complicated than that of a reaction dominated by a localized saddle point region or other localized topographical feature of a potential energy surfaces or set of potential energy surfaces.<sup>21</sup> The picturesque funnel language emphasizes the shape of the crossing in the two dimensions called the branching plane where the surfaces cross only at a point, but in many cases greater significance should be attached to the much larger number of dimensions in which the degeneracy is not broken. A picture describing how some coordinates break the degeneracy but others do not is an inverted cuspidal ridge rather than a funnel, or touching cuspidal ridges (an excited surface with ridge down and lower surface with ridge up, with the surfaces touching all along the ridges) rather than a bifunnel (a double cone, that is, a cone touching an inverted cone at a point).

The ACs are locations of nonzero minima in the energy gap as a function of local motion and are almost always associated with nearby CIs,<sup>20,22,23</sup> although those CIs may be energetically inaccessible. The most noteworthy WIs are characterized by wide regions of weak coupling between nearly parallel potential surfaces. Unlike CIs, there is no rule to prevent regions of coupling due to ACs and WIs from occurring in dimensionalities higher than  $F - 2$ . Although the edited volume in which this chapter appears focuses on CIs and their NBO dynamics, it is important to recognize that realistic potential energy surfaces featuring CIs contain chemically relevant nearby regions of ACs and may also contain regions of significant WIs. The methods presented in this chapter are general enough to treat all these cases.

The presence of a CI is often inferred when ultrafast decay is observed experimentally, and the CI is treated as a critical configuration connecting photoexcited reactants to quenched products when constructing mechanistic reaction coordinate diagrams of photochemistry. One can make a rough analogy to a transition state, but the analogy is at best imperfect and sometimes even deceptive because there are important differences between a CI and an adiabatic transition state as well as differences in the energetic accessibility of other critical regions of the potential energy surface in typical non-BO processes as compared to the kind of reaction where transition state theory is most useful.<sup>21</sup> Transition state dividing surfaces are of dimension  $F - 1$ , and valid transition state dividing surfaces are such that all of the reactive flux must cross through them. Due to the reduced dimensionality of CIs, on the other hand, only a vanishingly small fraction of electronically nonadiabatic flux passes through a CI at the zero-gap intersection. Furthermore, quantitative studies of electronically nonadiabatic systems

often require dynamical treatments that are more global than conventional transition state theories, and modeling multistate dynamics occurring via CIs is likely to require global dynamical methods as well. These considerations have motivated the development of trajectory-based methods for simulating NBO chemistry.

In NBO molecular dynamics, an ensemble of classical trajectories is used to model nuclear motions, electronic motion is treated quantum mechanically, and the nuclear and electronic subsystems are coupled according to semiclassical rules. Each trajectory in the ensemble may be thought of as representing a portion of a quantum mechanical wave packet, and taken together the evolution of the ensemble describes the flow of nuclear probability density over the coupled electronic surfaces. Alternatively, each trajectory in the ensemble may be thought of as a distinct chemical event, with its coordinates and momenta subject to the inherent indeterminacy of quantum mechanics.

NBO molecular dynamics is vulnerable to the same sources of error as conventional molecular dynamics, such as the errors associated with the neglect of tunneling through barriers, neglect of quantized vibrations and zero point energies, and neglect of coherences and resonances. NBO molecular dynamics is designed to incorporate one quantum mechanical effect into classical dynamics, namely that of the nonradiative electronic transitions. Accurate treatments of this quantum effect require consideration of tunneling and electronic coherence as well.

A variety of NBO molecular dynamics methods have been proposed. Here we discuss NBO molecular dynamics generally and focus our attention on two implementations: the fewest-switches with time uncertainty<sup>24</sup> (FSTU) surface hopping<sup>25–27</sup> method and the coherent switches with decay of mixing<sup>28</sup> (CSDM) method, a modification of the mean-field<sup>29–31</sup> formalism. The computational cost of these methods is close to that of conventional (i.e. electronically adiabatic) molecular dynamics, and the methods may be readily applied to study a wide variety of chemical processes in both small molecules and large ones.

The dynamics of each trajectory in an FSTU or CSDM ensemble is independent of the others, and transitions between electronic states are allowed anywhere that the electronic surfaces are coupled. Other classes of semiclassical NBO dynamics methods, such as those involving propagating coupled swarms of trajectories,<sup>32–34</sup> restricting hops to predetermined seams,<sup>25,26,35</sup> dressing classical trajectories with frozen Gaussians,<sup>36–40</sup> etc., are not considered in detail, nor are fully quantal calculations.<sup>41–45</sup>

The goal of this chapter is to describe in detail the latest implementations of the FSTU and CSDM methods, summarize the results of the tests used to validate and develop the methods, and describe several recent applications. Trajectory-based methods such as FSTU and CSDM are well suited for mechanistic interpretation, and a brief discussion of this application is also given.

## 2. Non-Born–Oppenheimer Molecular Dynamics

### 2.1. Coupled potential energy surfaces

In the NBO molecular dynamics simulations described here, an ensemble of independent classical trajectories for nuclear motion is propagated under the influence of a small number of coupled electronic states. The electronic energies (including nuclear repulsion) of each electronic state  $i$  provide a potential energy surface  $V_i$  for nuclear motion. When representing coupled electronic surfaces, one has a choice of electronic wave functions. The adiabatic electronic wave functions  $\varphi_i$  and energies  $V_i$  (where  $i$  labels the electronic states) are solutions of the electronic Schrödinger equation

$$H_0\varphi_i = V_i\varphi_i, \quad (1)$$

where  $H_0$  contains the electronic kinetic energy and the Coulomb potential operators. When solving Eq. (1), the nuclear coordinates  $\mathbf{Q}$  are treated parametrically, and  $V_i(\mathbf{Q})$  are the adiabatic potential energy surfaces.

The nuclear kinetic energy operator is written as

$$T_n = -\frac{\hbar^2}{2M}\nabla_n^2, \quad (2)$$

where  $\nabla_n$  is a  $3N$ -dimensional gradient in the nuclear coordinates  $\mathbf{Q}$ , which are scaled to common reduced mass  $M$  (for example,  $M$  could be 1 amu). The total wave function of the system is written

$$\Psi = \sum_i \varphi_i(\mathbf{q}; \mathbf{Q}) \chi_i(\mathbf{Q}), \quad (3)$$

where  $\mathbf{q}$  is the collection of electronic coordinates, and  $\chi_i$  is a wave function for nuclear motion.

If Eq. (3) is used to solve the full molecular Schrödinger equation with the Hamiltonian  $H = T_n + H_0$ , and if one neglects vibronic Coriolis coupling,

one obtains a set of coupled equations for the nuclear motion<sup>1,4,46</sup>

$$\left(T_n + V_i - \frac{\hbar^2}{2M}G_{ii} - E\right)\chi_i = -\sum_{j\neq i}\left(\frac{\hbar^2}{2M}\mathbf{F}_{ij}\cdot\nabla_n + \frac{\hbar^2}{2M}G_{ij}\right)\chi_j, \quad (4)$$

where  $G_{ii} = \langle\varphi_i|\nabla_n^2|\varphi_i\rangle$  are Born–Oppenheimer diagonal corrections (BODCs),<sup>47–50</sup>  $\mathbf{F}_{ij} = \langle\varphi_i|\nabla_n|\varphi_j\rangle$  are nonadiabatic coupling vectors,  $G_{ij} = \langle\varphi_i|\nabla_n^2|\varphi_j\rangle$  are 2nd-order nonadiabatic couplings, and Dirac brackets denote integration over the electronic variables. Although they are not necessarily negligible,  $G_{ii}$  and  $G_{ij}$  are often neglected, which is considered a semiclassical approximation, and this yields

$$(T_n + V_i - E)\chi_i = -\sum_{j\neq i}\frac{\hbar^2}{2M}\mathbf{F}_{ij}\cdot\nabla_n\chi_j. \quad (5)$$

Equation (5) is interpreted as coupling nuclear motion on the adiabatic surfaces  $V_i$  via the action of the nonadiabatic coupling vectors  $\mathbf{F}_{ij}$ .

Diabatic electronic wave functions may be generally defined as any linear combination of the adiabatic ones,<sup>51,52</sup>

$$\varphi_j^d = \sum_i d_{ij}\varphi_i, \quad (6)$$

that, unlike the adiabatic states, do not diagonalize  $H_0$ . Note that the  $d_{ij}$  are typically functions of  $\mathbf{Q}$ . The particular linear combination is often chosen such that the resulting diabatic potential energy surfaces

$$W_{ii} = \langle\varphi_i^d|E_0|\varphi_i^d\rangle \quad (7)$$

or diabatic states have some desirable property, such as smoothness. One may attempt to obtain to define a diabatic basis by minimizing the nonadiabatic coupling vectors; and the electronic basis where

$$\mathbf{F}_{ij}^d \equiv \langle\varphi_i^d|\nabla_n|\varphi_j^d\rangle = 0 \quad (8)$$

for all  $i$  and  $j$  is called the strictly diabatic basis. For real systems, no such strictly diabatic basis generally exists unless an infinite number of electronic states are considered.<sup>53</sup> The most useful diabatic states are those for which  $\mathbf{F}_{ij}^d$  is small enough to neglect and where the infinities in  $\mathbf{F}_{ij}$  associated with conical intersections have been transformed away. Such useful diabatic representations can be defined with manageable numbers of electronic states (even with only two). In the discussion that follows, we use “diabatic” both

to refer to the artificial situation where Eq. (8) is satisfied and also to refer to the more general situation where  $\mathbf{F}_{ij}^d$  is small and is neglected.

Some workers (including us at times) define the nonexistent set of diabatic states for which  $\mathbf{F}_{ij}^d$  vanishes identically as “strictly diabatic” and define the states where  $\mathbf{F}_{ij}^d$  is small or negligible as “quasidiabatic”. Here, as just mentioned, we use a simpler notation, which is also in common use, of just calling all such states “diabatic”. One should not think of “diabatic” as a synonym for “not adiabatic”; one could have states that are neither adiabatic nor diabatic. Such representations will be called “mixed”.

Diabatic electronic wave functions are not eigenfunctions of  $H_0$ , and in general

$$W_{ij} = \langle \varphi_i^d | H_0 | \varphi_j^d \rangle \neq 0 \quad (9)$$

for  $i \neq j$ . If we write

$$\Psi = \sum_i \varphi_i^d(\mathbf{q}; \mathbf{Q}) \chi_i(\mathbf{Q}), \quad (10)$$

then the equation governing nuclear motion in the diabatic representation is

$$(T_n + W_{ii} - E) \chi_i = \sum_{j \neq i} W_{ij} \chi_j, \quad (11)$$

where the off-diagonal matrix elements of the electronic Hamiltonian  $W_{ij}$  couple the nuclear motion on the diabatic surfaces  $W_{ij}$ , and we have taken advantage of the assumed negligibility of  $\mathbf{F}_{ij}^d$ .

It is straightforward to employ a general electronic basis, where  $\mathbf{F}_{ij}^d$  is not neglected and where  $W_{ij} \neq 0$ . This so-called mixed representation will not be explicitly considered, though the equations governing NBO dynamics in a mixed representation are straightforward extensions of the adiabatic and diabatic ones.

Adiabatic energies and couplings are readily calculated from the diabatic potential energy matrix elements  $W_{ij}$  and their gradients. The adiabatic energies  $V_i$  are the eigenvalues of the diabatic energy matrix  $\mathbf{W}$ , and the variables  $d_{ij}$  introduced already in Eq. (6) are the elements of a matrix whose columns are the eigenvectors of  $\mathbf{W}$ . The gradients of the adiabatic surfaces and the nonadiabatic couplings are

$$\nabla_n V_i = \sum_{j,k} d_{ij}^* d_{ik} \nabla_n W_{jk}, \quad (12)$$

$$\mathbf{F}_{ij} = \begin{cases} \frac{1}{V_j - V_i} \sum_{k,l} d_{ik}^* d_{jl} \nabla_n W_{kl} & (i \neq j) \\ 0 & (i = j). \end{cases} \quad (13)$$

On the other hand, if one knows the adiabatic energies and couplings, one may obtain diabatic energies and couplings, but due to the non-uniqueness of the diabatic representation, additional choices and approximations will be needed.<sup>54,55</sup> Procedures have also been developed for obtaining diabatic states without calculating the nonadiabatic coupling vectors.<sup>56–60</sup>

Spin-orbit coupling and other perturbative terms in the molecular Hamiltonian have not yet been considered. These terms may be readily treated using the dynamical methods to be described here, with one principal complexity being the need for a more complicated notation. When spin-orbit coupling is the dominant dynamical coupling and spin-free coupling is to be neglected, the adiabatic surfaces discussed above (which diagonalize the spin-free Hamiltonian  $H_0$  and may be called *valence-adiabatic states*<sup>61</sup>) are often a convenient diabatic basis for the full Hamiltonian, e.g. a useful diabatic matrix for a spin-orbit-coupled two-state system might be

$$\begin{pmatrix} V_1 & U_{\text{SO}} \\ U_{\text{SO}} & V_2 \end{pmatrix}, \quad (14)$$

where  $U_{\text{SO}}$  is the spin orbit coupling. The eigenvalues of Eq. (14) are the adiabatic potential energy surfaces for the full Hamiltonian including spin. It is equally straightforward to include both spin-free and spin-orbit coupling, as in a recent application to the photodissociation of HBr.<sup>62</sup>

Throughout the rest of this chapter, it is assumed that global potential energy surfaces and their gradients and couplings are available or may be readily calculated for all the electronic states of interest in either the diabatic or the adiabatic representations.

## 2.2. Efficient integration of NBO trajectories

An NBO trajectory evolves independently from the other trajectories in the ensemble and according to classical equations of motion

$$\dot{\mathbf{P}} = -\nabla_n \bar{V}(\mathbf{Q}), \quad (15)$$

$$\dot{\mathbf{Q}} = \mathbf{P}/M, \quad (16)$$

where  $\mathbf{P}$  is the vector of associated mass-scaled nuclear momenta, and the over-dot indicates time-differentiation. The time-dependence of  $\mathbf{Q}$  defines a path through configuration space, and when  $\bar{V}$  is the ground state adiabatic potential energy surface,  $\mathbf{Q}(t)$  is a conventional classical trajectory. More general formulations of  $\bar{V}$  are required to accurately model NBO nuclear-electronic coupling, as will be described in detail in Secs. 3 and 4 for the FSTU and CSDM methods.

The electronic state of the system at any time along an NBO trajectory may be represented as an electronic state density matrix with elements  $\rho_{ij}$  where the diagonal elements  $\rho_{ii}$  are the electronic populations of states  $i$  and the off-diagonal elements  $\rho_{ij}$  are coherences. The time evolution of the electronic density matrix  $\rho_{ij}$  is obtained by solving semiclassical equations along each NBO trajectory; this is sometimes called the classical path approximation. This approach is equivalent to solving for the quantum dynamics of the electronic subsystem in a time-dependent field, which in the present context is created by the nuclear motion. The electronic wave function may be expanded in the adiabatic basis

$$\Phi = \sum_i c_i \varphi_i, \quad (17)$$

where  $c_i = a_i + ib_i$  are complex time-dependent expansion coefficients, and the electronic density matrix is defined by

$$\rho_{ij} = c_i^* c_j. \quad (18)$$

The evolution in time of  $\Phi$  is obtained in this section by solving the time-dependent electronic Schrödinger equation

$$i\hbar \frac{\partial}{\partial t} \Phi = H_0 \Phi, \quad (19)$$

giving the classical path equation:

$$\dot{c}_i = -i\hbar^{-1} c_i V_i - \sum_j c_j \dot{\mathbf{Q}} \cdot \mathbf{F}_{ij}, \quad (20)$$

or, for the real and imaginary parts of  $c_i$ ,

$$\dot{a}_i = \hbar^{-1} b_i V_i - \sum_j a_j \dot{\mathbf{Q}} \cdot \mathbf{F}_{ij}, \quad (21)$$

$$\dot{b}_i = -\hbar^{-1} a_i V_i - \sum_j b_j \dot{\mathbf{Q}} \cdot \mathbf{F}_{ij}, \quad (22)$$

where  $\dot{\varphi}_i$  was evaluated using the “chain rule”<sup>63</sup>

$$\dot{\varphi}_i = \dot{\mathbf{Q}} \cdot \nabla_n \varphi_i, \quad (23)$$

which is a semiclassical approximation. If a diabatic basis is used,

$$\Phi = \sum_i c_i^d \varphi_i^d, \quad (24)$$

and

$$\dot{c}_i^d = -i\hbar^{-1} \sum_j c_j^d W_{ij}. \quad (25)$$

or

$$\dot{a}_i^d = \hbar^{-1} \sum_j b_j^d W_{ij}, \quad (26)$$

$$\dot{b}_i^d = -\hbar^{-1} \sum_j a_j^d W_{ij}. \quad (27)$$

The time-dependence in Eqs. (20) and (25) contains an arbitrary phase factor that spins rapidly due to the action of  $V_i$  or  $W_{ii}$  on  $\dot{c}_i$  or  $\dot{c}_i^d$ . This phase is readily analytically removed to simplify integration of the electronic variables by writing

$$c_i = \tilde{c}_i \exp(-i\theta_i), \quad (28)$$

where

$$\theta_i = \int V_i dt, \quad (29)$$

or

$$c_i^d = \tilde{c}_i^d \exp(-i\theta_i^d) \quad (30)$$

and

$$\theta_i^d = \int W_{ii}^d dt. \quad (31)$$

These substitutions give

$$\dot{\tilde{a}}_i = - \sum_{j \neq i} [\cos(\theta_j - \theta_i) \tilde{a}_j + \sin(\theta_j - \theta_i) \tilde{b}_j] \dot{\mathbf{Q}} \cdot \mathbf{F}_{ij}, \quad (32)$$

$$\dot{\tilde{b}}_i = - \sum_{j \neq i} [\cos(\theta_j - \theta_i) \tilde{b}_j - \sin(\theta_j - \theta_i) \tilde{a}_j] \dot{\mathbf{Q}} \cdot \mathbf{F}_{ij}, \quad (33)$$

and

$$\dot{\tilde{a}}_i^d = - \sum_{j \neq i} [\sin(\theta_j^d - \theta_i^d) \tilde{a}_j^d - \cos(\theta_j^d - \theta_i^d) \tilde{b}_j^d] W_{ij}, \quad (34)$$

$$\dot{\tilde{b}}_i^d = - \sum_{j \neq i} [\sin(\theta_j^d - \theta_i^d) \tilde{b}_j^d + \cos(\theta_j^d - \theta_i^d) \tilde{a}_j^d] W_{ij}. \quad (35)$$

Equation (20) neglects vibronic Coriolis coupling, which is discussed elsewhere.<sup>3</sup> In addition, it neglects electronic angular momentum.

It is straightforward to write equations for the time-dependence of the elements of the electronic density matrix by differentiating Eq. (18) and using Eqs. (20) or (25):

$$\dot{\rho}_{ij} = i\hbar^{-1}(\rho_{ii}V_{ii} - \rho_{jj}V_{jj}) + \sum_k \rho_{ik} \dot{\mathbf{Q}} \cdot \mathbf{F}_{ik} - \rho_{kj} \dot{\mathbf{Q}} \cdot \mathbf{F}_{kj}, \quad (36)$$

$$\dot{\rho}_{ij}^d = -i\hbar^{-1} \sum_k \rho_{ik}^d W_{ik} - \rho_{kj}^d W_{kj}. \quad (37)$$

The off-diagonal elements of  $\rho_{ii}$  are complex, and the real and imaginary parts must be integrated separately. The equations for the (real) electronic state populations may be further simplified

$$\dot{\rho}_{ii} = -2 \sum_{j \neq i} \text{Re}(\rho_{ij} \dot{\mathbf{Q}} \cdot \mathbf{F}_{ik}), \quad (38)$$

$$\dot{\rho}_{ii}^d = 2\hbar^{-1} \sum_{j \neq i} \text{Im}(\rho_{ij}^d W_{ik}). \quad (39)$$

Quantum mechanical calculations without dynamical approximations and some NBO molecular dynamics methods are independent of the choice of electronic representation if no coupling terms are neglected. In general though, NBO simulations will be dependent on the choice of electronic representation, and both representations will be considered when the FSTU and CSDM methods are described in Secs. 3 and 4. Propagating an NBO trajectory for a system with  $N$  electronic states requires integrating the nuclear equations of motion [Eqs. (15) and (16)], as well as either the  $2N$  real and imaginary parts of the adiabatic or diabatic electronic coefficients  $c_i$  [Eqs. (32) and (33) or (34) and (35)] and the  $N$  phases [Eqs. (29) or (31)] or the  $N^2$  unique real and imaginary elements of the adiabatic or diabatic electronic density matrix  $\rho_{ij}$  [Eqs. (36) and (38) or (37) and (39)].

Although Eqs. (5) and (11) coupled to Eq. (20), (25), (36), or (37) are derived from the accurate Eqs. (4) and (19), the process of treating the

nuclear equations of motion classically means that the quantum electronic subsystem is no longer explicitly coupled to a quantum mechanical environment. It is not correct to treat the electronic subsystem by eq 19 because it is not an isolated system; Eq. (19) is valid only for isolated systems. For subsystems coupled to a medium or environment, one must replace the time-dependent Schrödinger equation [Eq. (19)] by a nonunitary Liouville–von Neumann equation.<sup>64–66</sup> Here the system consists of the electronic degrees of freedom, and the medium consists of the nuclear degrees of freedom; the “nuclear degrees of freedom play the role of observers of the electronic degrees of freedom.”<sup>66</sup> The effects of the medium may be broadly described as decoherence.<sup>65–70</sup> The effect of decoherence will be treated by a simple model<sup>71</sup> in Sec. 3 and by a more complete model<sup>8,28,65</sup> in Sec. 4.

### 2.3. *Initial conditions for photochemistry*

The ensemble of NBO trajectories is initiated with some distribution in coordinate and momentum space that is intended to simulate the width (or uncertainty) of a quantum mechanical wave packet or of a single-energy slice through a wave packet. The type of reaction and/or experimental situation being modeled determines the specific prescription for the selection of the initial conditions for each trajectory in the ensemble, and the techniques developed for single surface reaction dynamics<sup>72–75</sup> can be applied with minor modifications.

In one typical experimental situation, a chemical system is photoexcited from a well-characterized vibrational state of the ground electronic state to some excited target electronic state. A rigorous sampling scheme might involve calculating absorption cross sections<sup>76,77</sup> for the transitions of interest and sampling from the resulting distribution of quantized vibrational states of the excited electronic state or states. For systems with more than a few atoms the approximate methods used to calculate the ground state and excited state energy levels and the photoabsorption cross sections are likely to have significant uncertainty and/or computational cost.

A more efficient strategy for modeling this experimental situation and one that is likely suitable for NBO molecular dynamics of complex systems is as follows. One selects the initial nuclear coordinates and momenta from the ground-state wave function of interest using quasiclassical<sup>73,74</sup> initial conditions and then instantaneously promotes the trajectory to the target excited state. This scheme is equivalent to the Franck principle<sup>78</sup> (the semi-classical analog of the Franck–Condon principle); and it corresponds to

exciting the sampled ground state wave function with “white light” that will generally result in an ensemble of trajectories with a relatively wide range of total energies.

An alternative to using quasiclassical initial conditions is to run a classical trajectory (often called molecular dynamics) on the ground-electronic state adiabatic surface and sample from that trajectory. This is done by several groups. One should note, however, that a purely classical trajectory does not retain the quantum distribution of zero point energy or thermal or state-specific vibrational excitation energy in the various vibrational modes, except in the limit of vanishingly small vibrational motion. Therefore the quasiclassical initial conditions are preferred.

If the NBO dynamics are expected to be sensitive to energetic thresholds, it may be more appropriate to restrict the range of total energies. An alternative approach is to excite only that slice of the ground-state ensemble with energy gaps between the ground and target electronic states equal to the simulated photon energy within some tolerance. This scheme produces an arbitrarily narrow range of total energies, but it also limits the sampled configuration space.

When the initial conditions are selected from distributions associated with uncoupled regions of the potential energy surfaces, the electronic energies are independent of the choice of electronic representation and the initial electronic state may be assigned unambiguously. However, if an NBO simulation starts in a region where the initial electronic state is coupled to other electronic states, one has to choose both the initial electronic representation and the initial electronic state distribution. For example, it may be appropriate to compute initial distributions in the adiabatic representation. If the simulation is to be carried out in the diabatic representation, the initial adiabatic state  $i$  can be projected onto the diabatic states, with the initial diabatic state  $j$  selected with the weights  $d_{ij}^2$  obtained from the adiabatic-to-diabatic transformation.

Although quasiclassical initial conditions are quite reasonable for modeling excited vibrational states, they are qualitatively incorrect for ground vibrational states.<sup>79</sup> Thus one reasonable strategy<sup>80</sup> for photodissociation is to use Wigner distributions<sup>77</sup> for vibrational modes with vibrational quantum number 0 and quasiclassical distributions for vibrational modes with quantum number greater than 0. Wigner distributions may also be more accurate than quasiclassical initial conditions for bimolecular collisions,<sup>81,82</sup> but they are only accurate for a short time,<sup>83</sup> and their higher quantum fidelity may be lost by the time the collision partners meet.

### 3. Fewest Switches with Time Uncertainty

The dynamics methods presented here may be applied in either an adiabatic or a diabatic representation. The results of accurate quantum mechanical calculations and *some* NBO molecular dynamics calculations are independent of the choice of electronic representation. In general, however, as already mentioned in Sec. 2.2, surface hopping and decay of mixing NBO molecular dynamics simulations carried out using the adiabatic representation will produce different results from those employing diabatic representations. When the equations governing the NBO molecular dynamics methods depend on the choice of electronic representation, two equations will be given with the equation numbers appended with “a” and “d” for the adiabatic and diabatic representations, respectively.

Trajectory surface hopping was first employed by Bjerre and Nikitin.<sup>25</sup> Shortly thereafter it was presented in more generality by Preston and Tully.<sup>26</sup> The generalization to allow hopping at any location was first turned into a general algorithm by Blais and Truhlar,<sup>27</sup> as discussed in the excellent review of Chapman.<sup>84</sup> Then Tully improved this procedure by introducing the fewest switches algorithm.<sup>63</sup> The method we will present below differs from the original fewest switches algorithm in three ways: (i) the introduction of time uncertainty,<sup>24</sup> leading to the FSTU method, (ii) the use of a grad  $V$  algorithm,<sup>85</sup> and (iii) the introduction of stochastic decay<sup>71,86</sup> (SD). The SD modification in the FSTU/SD method is similar to the method recently employed by Granucci and Persico.<sup>70</sup> These three enhancements to the method are explained in detail below.

In a surface hopping simulation, such as an FSTU simulation, trajectories are propagated under the influence of a single adiabatic or diabatic electronic surface which, for electronic state  $K$ , is given by

$$\bar{V} = V_K, \quad (40a)$$

$$\bar{V} = W_{KK}, \quad (40d)$$

but this propagation is interrupted by instantaneous surface switches, i.e. the state label  $K$  in Eq. (40), which denotes the currently occupied electronic state, changes at certain points along the trajectory. A change in  $K$  is called a surface hop, and at a hopping event the trajectory is instantaneously placed on a different potential energy surface. In general, the potential energy  $\bar{V}$  will change discontinuously at a surface hop, and the

kinetic energy is adjusted such that total energy and total nuclear angular momentum are conserved. (Electronic angular momentum is neglected.) The nuclear momenta after the hop  $\mathbf{P}'$  from surface  $K$  to surface  $K'$  are given by

$$\mathbf{P}' = \mathbf{P} - \mathbf{P} \cdot \hat{\mathbf{h}}_{KK'} (1 - \sqrt{1 - \Delta_{KK'}/T_{KK'}}) \hat{\mathbf{h}}_{KK'}, \quad (41)$$

where  $\hat{\mathbf{h}}_{KK'}$  is a unit vector called the hopping vector,

$$\Delta_{KK'} = V_{K'} - V_K, \quad (42a)$$

$$\Delta_{KK'} = W_{K'K'} - W_{KK}, \quad (42d)$$

and

$$T_{KK'} = \frac{1}{2M} (\mathbf{P} \cdot \hat{\mathbf{h}}_{KK'})^2 \quad (43)$$

is the nuclear kinetic energy associated with  $\hat{\mathbf{h}}_{KK'}$ . The hopping vector determines the component of the nuclear momentum that is adjusted during a hop, and theoretical arguments<sup>26,87</sup> confirmed by numerical tests<sup>42</sup> show that a good choice is

$$\hat{\mathbf{h}}_{KK'} = \mathbf{F}_{KK'} / |\mathbf{F}_{KK'}|. \quad (44a)$$

Because  $\mathbf{F}_{KK'}$  is a vector of internal coordinates, the adjustment in Eq. (41) with the choice of Eq. (44a) conserves total angular momentum.

Using the nonadiabatic coupling vector as the hopping vector has been shown to provide accurate results for surface hopping calculations carried out in both the adiabatic and diabatic representations.<sup>42</sup> If the diabatic representation is used,  $\mathbf{F}_{KK'}$  can be calculated directly from Eq. (13) for a two-state system. When more than two states are involved,  $\mathbf{F}_{KK'}$  should not be used because the adiabatic and diabatic state labels do not generally correlate to a globally consistent pair of states. Instead, the hopping vector in the diabatic representation can be approximated as

$$\hat{\mathbf{h}}_{KK'} = \mathbf{F}_{KK'}^r / |\mathbf{F}_{KK'}^r|, \quad (44d)$$

where  $\mathbf{F}_{KK'}^r$  is the reduced nonadiabatic coupling for the submatrix

$$\mathbf{W}^r = \begin{pmatrix} W_{KK} & W_{KK'} \\ W_{K'K} & W_{K'K'} \end{pmatrix}, \quad (45)$$

i.e.,

$$\mathbf{F}_{KK'}^r = \frac{d_{KK}^{r,*} d_{K'K}^r \nabla_n W_{KK} + (d_{KK}^{r,*} d_{K'K'}^r + d_{KK'}^{r,*} d_{K'K}^r) \nabla_n W_{KK'} + d_{KK'}^{r,*} d_{K'K'}^r \nabla_n W_{K'K'}}{W_+ - W_-}, \quad (46)$$

and  $W_+$  and  $W_-$  are the eigenvalues, and  $d_{KK'}^r$  are the elements of matrices whose columns are the eigenvectors of  $\mathbf{W}^r$  defined by Eq. (45).

Equation (41) cannot be solved if the radicand is negative, i.e. if the kinetic energy associated with the hopping vector is less than the required energy adjustment and the hop is an upward hop. (For downward hops,  $\Delta_{KK'} < 0$  and Eq. (41) can always be solved.) When  $\Delta_{KK'} > T_{KK'}$ , the hop is declared “frustrated”, and additional considerations are required, as discussed in detail below.

In early examples of trajectory surface hopping, hops were allowed only when a trajectory crossed a seam where  $W_{KK}$  crosses another diabatic surface,<sup>25,26</sup> but in later work<sup>27,63</sup> this was generalized so that stochastic hopping events may occur after each integration step  $\Delta t$  and anywhere along the trajectory where the currently occupied surface is coupled to one or more other surfaces. Tully provided an elegant and useful formulation<sup>63</sup> for the probability for hopping from the currently occupied electronic state  $K$  to some other state  $K'$

$$P_{KK'}(t + \Delta t) = \max \left\{ \begin{array}{l} - \int_{t'=t}^{t+\Delta t} dt' b_{KK'}(t') / \rho_{KK}(t) \\ 0 \end{array} \right. , \quad (47)$$

where

$$b_{KK'} = -2\text{Re}(\rho_{KK'} \dot{\mathbf{Q}} \cdot \mathbf{F}_{KK'}), \quad (48a)$$

$$b_{KK'} = 2\hbar^{-1} \text{Im}(\rho_{KK'}^d W_{KK'}). \quad (48d)$$

Equation (47) is the relative rate of change of the electronic population of state  $K$  due to coupling to the state  $K'$ . Hops away from state  $K$  are allowed only if  $\rho_{KK}$  is decreasing, and Eq. (47) is designed to maintain the populations of trajectories in each electronic state  $n_i$  according to  $\rho_{ii}$  with the fewest number of hops. (The self consistency of  $n_i$  and  $\rho_{ii}$  is generally *not* maintained, as discussed below.) Equation (47) is called the fewest switches (FS) hopping probability, and this scheme is also called molecular dynamics with quantum transitions (MDQT), which can be confusing because it is not the only scheme for molecular dynamics with quantum transitions.

The quantity  $B_{KK'}(t) = \int_{t'=0}^t b_{KK'}(t')dt'$  can be integrated along with the nuclear and electronic variables, such that the hopping probability at time  $t + \Delta t$  may be evaluated as

$$P_{KK'}(t + \Delta t) = \max \left\{ \begin{array}{l} [B_{KK'}(t + \Delta t) - B_{KK'}(t)] / \rho_{KK}(t) \\ 0 \end{array} \right. . \quad (49)$$

Because surface hops are only allowed between time steps, and because hopping and nonhopping trajectories diverge from one another, the results of a surface hopping simulation must be converged with respect to the available hopping locations. Often, quite small step sizes are required when the electronic populations are changing rapidly, whereas larger step sizes (ultimately limited by the accuracy of the integration of the nuclear coordinates) may be used when propagating through uncoupled regions of potential surface. This situation benefits from variable-step-size integrators.

It may be difficult to converge the available hopping locations when using efficient adaptive-step-size integrators, as the integrator may step through regions where  $\rho_{KK'}$  changes sign. Consider an example where a large step  $\Delta t$  is taken through a region where  $\rho_{KK}$  is locally quadratic and where  $\rho_{KK}(t) = \rho_{KK}(t + \Delta t)$ . The FS hopping probability for this step is 0, whereas if two steps of size  $\Delta t/2$  are taken, the hopping probability will be finite for one of the steps. Many variable step size integrators can integrate quadratic functions exactly, and this example is of practical concern. A simple modification<sup>42</sup> provides a solution. Specifically, if the increasing

$$b_{KK'}^+ = \max(b_{KK'}, 0) \quad (50)$$

and decreasing

$$b_{KK'}^- = \min(b_{KK'}, 0) \quad (51)$$

parts of  $b_{KK'}$  are integrated separately, the integrator is made to take small steps where  $b_{KK'}$  changes sign and where  $b_{KK'}^+$  and  $b_{KK'}^-$  have discontinuous derivatives.

As mentioned above, the FS hopping probability attempts to populate the various electronic states with trajectories such that the fractions of trajectories in each electronic state  $n_i \approx \rho_{ii}$  (with the accuracy limited by the finite number of trajectories that are sampled). This self consistency is maintained only when trajectories in the various electronic states do not

diverge from one another, i.e. when the potential surfaces are degenerate. For real potential energy surfaces, trajectories in different electronic states diverge, and self consistency is not preserved, although it may be maintained in an ensemble averaged sense, i.e.  $n_i \approx \langle \rho_{ii} \rangle$ , where the brackets denote an average over the members of the ensemble of trajectories. When classically forbidden hops occur, only upward hops can be frustrated, and self consistency cannot be maintained.<sup>88,89</sup>

One may distinguish two sources of frustrated hops in trajectory simulations. First, the FS algorithm may be incomplete in some way that is causing it to predict finite hopping probabilities where hops should not be allowed. This argument is strengthened by studies showing that accurate results may sometimes be obtained when frustrated hops are simply ignored.<sup>90</sup> As pointed out in the original formulation<sup>63</sup> and further developed in later work,<sup>28,65–71,91,92</sup> one deficiency of the original FS method and other methods based on classical path electronic dynamics is that decoherence is not treated. (We will see below that including decoherence may reduce the number of frustrated hops by reducing unphysical amplitudes for unoccupied states in regions when such states are no longer strongly coupled.) Another possibility is that the FS method is correctly predicting energetically forbidden surface hops, but the hops are frustrated due to the limitations of classical mechanics. In this picture, a frustrated hop is a quantum mechanical attempt to tunnel into a classically forbidden region of an excited electronic state. Several improvements to the FS method based on both of the latter two considerations have been developed and are discussed in the remainder of this section.

One suggestion that was made for eliminating frustrated hops is to use modified velocities for the integration of the quantum amplitudes.<sup>88,92</sup> We do not employ this because comparison to accurate quantum dynamics shows<sup>89</sup> that it decreases the accuracy as compared to using the original unmodified velocities.

The first improvement to the FS method that we discuss is a simple modification designed to incorporate decoherence.<sup>71</sup> Prior to the first surface hop, the electronic variables are assumed to correctly evolve coherently along the trajectory according to the classical path equations. At a surface hop or an attempted surface hop, the system is imagined to split into two wave packets, one traveling on each of the surfaces involved in the surface hop. The system immediately begins to decohere with a first-order rate coefficient  $\tau_{\text{SD}}^{-1}$  obtained by considering the short time evolution of the overlap of two one-dimensional wave packets traveling in the different

electronic states<sup>93</sup>

$$\tau_{\text{SD}}^{-1} = \frac{\pi}{2} \frac{\Delta f_{KK'}}{\bar{p}_{KK'}} + \sqrt{\left(\frac{\Delta p_{KK'}}{h}\right)^2 \frac{\Delta_{KK'}}{M} + \left(\frac{\pi \Delta f_{KK'}}{2\bar{p}_{KK'}}\right)^2}, \quad (52)$$

where

$$f_{KK'} = -\nabla_n(V_K - V_{K'}) \cdot \hat{\mathbf{h}}_{KK'} \quad (53)$$

is the difference in the forces of the two electronic states in the direction of the hopping vector,

$$\Delta p_{KK'} = (\mathbf{P} - \mathbf{P}') \cdot \hat{\mathbf{h}}_{KK'} \quad (54)$$

is the difference in the nuclear momenta before and after the surface hop in the direction of the hopping vector, and

$$\bar{p}_{KK'} = \frac{1}{2}(\mathbf{P} + \mathbf{P}') \cdot \hat{\mathbf{h}}_{KK'}. \quad (55)$$

If the decoherence event is initiated at a frustrated hop,  $\mathbf{P}'$  cannot be calculated and is set to zero in Eqs. (54) and (55).

At each time step (of step size  $\Delta t$ ) after the frustrated or successful hop, a stochastic decoherence (SD) probability is computed

$$P_{\text{SD}}(\Delta t) = \exp(-\Delta t/\tau_{\text{SD}}), \quad (56)$$

and  $P_{\text{SD}}$  is compared to a random number between 0 and 1. If the SD check is successful, the electronic state density matrix is reset to

$$\rho_{ij} = \begin{cases} 1 & \text{for } i, j = K, \\ 0 & \text{otherwise,} \end{cases} \quad (57)$$

where  $K$  is the currently occupied electronic state. After reinitialization, the electronic state populations evolve according to the coherent classical path equations. If a frustrated or successful hop occurs before decoherence is called for,  $\tau_{\text{SD}}$  is updated and decoherence checks are continued.

The SD algorithm damps out coherence after some physically motivated time, which reduces the likelihood of the FS algorithm calling for surface hops in regions of weak coupling that are encountered between regions of strong coupling. This has the practical and intended physical effect of reducing frustrated hops in regions where the potential energy surfaces have

different energies and/or shapes; decoherence is expected to be fast in such regions.

The next improvement to the FS method incorporates time-uncertainty (TU) hopping,<sup>24</sup> which simulates tunneling into classically forbidden regions of excited electronic states. Inspired by the time-energy version of the uncertainty principle, a frustrated hop occurring at some time  $t_f$  is allowed to hop at the nearest time  $t_h$  along the trajectory where a hop would be energetically allowed (if such a time exists) but only if

$$|t_f - t_h| \leq \hbar/2E_{\text{def}}, \quad (58)$$

where

$$E_{\text{def}} = \Delta_{KK'}(t_f) - T_{KK'}(t_f) \quad (59)$$

is the energy deficiency by which the attempted hop is frustrated. In this way, a TU hop may be thought of as allowing the trajectory to borrow an energy of  $E_{\text{def}}$  for some short time according to the uncertainty principle as it hops into the excited state. The FS method with TU hops was shown to significantly improve the accuracy of the surface hopping method for some systems, especially those with weakly coupled electronic surfaces.<sup>24</sup>

The FSTU method and the SD algorithm do not eliminate all frustrated hops. The remaining frustrated hops [i.e. those where a  $t_h$  satisfying Eq. (58) cannot be found] are attributed to the breakdown of the independent-trajectory approximation and are treated using the “grad  $V$ ” prescription.<sup>85</sup> In the method, a frustrated trajectory instantaneously receives an impulse from the classically forbidden electronic state based on its gradient in the direction of the hopping vector. Specifically, at a frustrated hop that cannot be remedied by the TU method, the components of the nuclear momentum and force in the target electronic state in the direction of  $\hat{\mathbf{h}}_{KK'}$  are calculated by

$$p_{K'} = \mathbf{P} \cdot \hat{\mathbf{h}}_{KK'}, \quad (60)$$

$$f_{K'} = -\nabla_n V_{K'} \cdot \hat{\mathbf{h}}_{KK'}, \quad (61a)$$

$$f_{K'} = -\nabla_n W_{K'K'} \cdot \hat{\mathbf{h}}_{KK'}. \quad (61d)$$

If  $p_{K'}$  and  $f_{K'}$  have the same sign, the influence of the target electronic state is to accelerate the trajectory, and we choose to continue the trajectory in the currently occupied electronic state without making any adjustments

to the nuclear momenta. If  $p_{K'}$  and  $f_{K'}$  have different signs, the target electronic state is thought to “reflect” the trajectory, and we choose to continue the trajectory in the currently occupied electronic state with the nuclear momentum reversed in the direction of  $\hat{\mathbf{h}}_{KK'}$ , i.e.

$$\mathbf{P}'' = \mathbf{P} - 2\mathbf{P} \cdot \hat{\mathbf{h}}_{KK'} \hat{\mathbf{h}}_{KK'}. \quad (62)$$

If the probability of an electronically inelastic event is very small because the probability of a hop is very small, e.g.  $10^{-6}$ , it would typically require very extensive sampling to observe even one inelastic event and even more sampling to accumulate good statistics. For such cases special methods of rare-event sampling have been developed.<sup>94</sup>

It is interesting to examine the question of whether surface hopping methods can be improved by replacing the trajectories with wave packets. In principle the answer is yes, but so far no generally affordable method for doing so has been devised. The most widely employed method involving wave packets for photochemical calculations is the full multiple spawning (FMS) method.<sup>36–39</sup> The assumptions underlying this method have been examined in detail.<sup>37</sup> It was stated<sup>37</sup> that the basis set expansion method underlying FMS “is aimed only at describing quantum mechanical effects associated with electronic nonadiabaticity and *not* at correcting the underlying classical dynamics.” One of many serious approximations in replacing an ensemble of trajectories with an ensemble of wave packets is that the wave packets must be coupled. In FMS, in order to keep the method practical, interference between the various initial wave packets that are required<sup>95</sup> to simulate the initial quantum state is neglected; this serious approximation is called the independent-first-generation approximation.<sup>37</sup> One of the features that makes trajectory calculations affordable for complex systems is that an ensemble of trajectories can be run independently of each other, without introducing approximations to accurate classical mechanics. In contrast, running wave packets independently is a serious approximation that is not overcome by spawning more packets or spawning them in a more physical way. Furthermore, FMS does not include decoherence in the treatment of electronic nonadiabaticity (it uses a unitary treatment of the electronic degrees of freedom, not a nonunitary one<sup>65</sup> as in the CSDM method discussed in the next section). Thus FMS is expected to have about the same accuracy as surface hopping without decoherence, which is consistent with our numerical tests.

Efforts to derive improved wave packet methods are underway in more than one group.<sup>40,96</sup> The reader is also referred to the multiconfiguration

time-dependent Hartree method,<sup>43–45</sup> which is a variational time-dependent wave function expansion method designed to achieve converged quantum dynamics in an efficient way; it has had outstanding success for small enough systems and systems with particularly amenable Hamiltonians.

#### 4. Coherent Switches with Decay of Mixing

One major deficiency of the FSTU method and of surface hopping methods in general is that the results of the NBO simulation may depend strongly on the choice of electronic representation, that is, adiabatic, diabatic, or mixed. Here we consider an alternative approach to NBO molecular dynamics based on a mean-field approximation. In its simplest form, the mean-field approximation under consideration here<sup>29–31</sup> is called the semiclassical Ehrenfest or SE approximation. It defines the semiclassical potential energy as a weighted average of the potential energy surfaces

$$\begin{aligned}\bar{V} &\equiv \langle \Phi | H_0 | \Phi \rangle \\ &= \sum_i \rho_{ii} V_{ii}\end{aligned}\quad (63a)$$

$$= \sum_{i,j} \text{Re}(\rho_{ij}^d) W_{ij}.\quad (63d)$$

Note that the gradient of the diabatic mean field energy is straightforward

$$\nabla \bar{V} = \sum_{i,j} \rho_{ij}^d \nabla W_{ij},\quad (64d)$$

whereas the gradient of the adiabatic mean field energy is

$$\nabla \bar{V} = \sum_i \rho_{ii} \nabla V_i + 2 \sum_{i \neq j} \text{Re}(\rho_{ij}) V_i \mathbf{F}_{ij},\quad (64a)$$

with the second term on the right hand side arising semiclassically from the action of the nuclear gradient on  $\rho_{ij}$ .<sup>97</sup> More rigorous derivations of the equations governing mean-field motion in the adiabatic representation equivalent to Eq. (64a) have been given.<sup>29</sup> SE trajectories are independent of the choice of electronic representation.

In the SE model, trajectories propagating through regions of coupling are governed by an effective potential energy surface that is evolving as an

appropriately weighted average of the coupled potential energy surfaces. Although this situation may be an accurate description of coupled-states semiclassical motion, a severe deficiency of the approach is that the trajectory remains in a coherent mixed state after the system leaves the region of coupling. This causes the SE method to predict molecular products to be in coherent superpositions of electronic states, which do not correspond to quantum mechanical or experimentally measured final states. Another less obvious but equally troubling consequence of fully coherent SE propagation is that the system does not “reset” electronically between regions of coupling, which may introduce errors into the dynamics.<sup>91,92</sup> Finally, SE trajectories are not able to explore some processes occurring with small probabilities, as the potential felt by an SE trajectory will be determined mainly by the potential energy surface associated with the higher-probability event.

The CSDM method<sup>28</sup> is a modification of the SE method designed to introduce decoherence outside regions of strong coupling, such that the predicted molecular products are formed in quantized final electronic states. As mentioned in Sec. 2.2, decoherence in the electronic equations of motion may be thought of as arising from the nuclear degrees of freedom acting as a bath, and the bath relaxes the electronic density matrix. An important feature of CSDM trajectories is that they behave similarly to SE trajectories in strong coupling regions, thus preserving much of the representation independence of the SE method.

The decay-of-mixing (DM) formalism collapses a coherent mixed state density matrix to a quantized pure state smoothly over time, and it includes both dephasing

$$\rho_{ij} \rightarrow 0 \quad (i \neq j) \quad (65)$$

and demixing

$$\rho_{ii} \rightarrow \delta_{iK}, \quad (66)$$

where  $\delta_{iK}$  is the Kronecker delta, and  $K$  labels the target decoherent state toward which the system is collapsing. The target decoherent state label  $K$  may change over time, as discussed below. When the electronic density matrix collapses to a quantized electronic state, the semiclassical potential energy surface [Eq. (63)] collapses to a pure one, thus providing realistic product internal energy distributions that may be compared with experimental and quantum mechanical ones.

Note that dephasing (as it is defined here as the damping of the off-diagonal elements of  $\rho_{ij}$ ) is a physical effect, whereas demixing is a semi-classical choice. Dephasing and demixing are assumed to occur at the same rate  $\tau_{iK}^{-1}$ , where

$$\tau_{iK} = \frac{\hbar}{|\Delta_{iK}|} \left( 1 + \frac{E_0}{(\mathbf{P} \cdot \hat{\mathbf{s}}_i)^2 / 2M} \right), \quad (67)$$

where each state  $i$  other than  $K$  has its own decoherence time  $\tau_{iK}$ ,  $E_0$  is a parameter typically chosen to be  $0.1 E_h = 2.72 \text{ eV}$ , and  $\hat{\mathbf{s}}_i$  is a unit vector called the decoherence vector. The decay time in Eq. (67) has a different functional form than the one used previously for the SD method [Eq. (52)] due to algorithmic requirements of the DM method. Equations (52) and (67) are expected to have similar magnitudes.<sup>93</sup> Alternatives to Eq. (67) have also been explored for CSDM calculations, and the results are not overly sensitive to the functional form.<sup>98</sup>

Decoherence and demixing are introduced into the NBO molecular dynamics by modifying the classical path electronic equations of motion,<sup>28,67</sup>

$$\dot{c}_i^{\text{DM}} = \dot{c}_i + \dot{c}_i^{\text{D}}, \quad (68)$$

where

$$\begin{aligned} \dot{c}_i^{\text{D}} &= \frac{1}{2} \frac{c_i}{\tau_{iK}} & i \neq K \\ &= \frac{1}{2} \frac{c_K}{\rho_{KK}} \sum_{j \neq K} \frac{\rho_{jj}}{\tau_{jK}} & i = K \end{aligned} \quad (69)$$

Equivalently, one may write the decoherence terms for the density matrix,

$$\dot{\rho}_{ij}^{\text{DM}} = \dot{\rho}_{ij} + \dot{\rho}_{ij}^{\text{D}}, \quad (70)$$

where

$$\begin{aligned} \dot{\rho}_{ii}^{\text{D}} &= -\frac{\rho_{ii}}{\tau_{iK}} & i \neq K \\ &= \sum_{j \neq K} \frac{\rho_{jj}}{\tau_{jK}} & i = K \end{aligned} \quad (71)$$

for the diagonal elements, and

$$\begin{aligned}\dot{\rho}_{ij}^{\text{D}} &= -\frac{1}{2} \left( \frac{1}{\tau_{iK}} + \frac{1}{\tau_{jK}} \right) \rho_{ij} & i, j \neq K \\ &= \frac{1}{2} \left( \frac{1}{\rho_{KK}} \sum_{k \neq K} \frac{\rho_{kk}}{\tau_{kK}} - \frac{1}{\tau_{jK}} \right) \rho_{ij} & i = K, j \neq K \\ &= \frac{1}{2} \left( \frac{1}{\rho_{KK}} \sum_{k \neq K} \frac{\rho_{kk}}{\tau_{kK}} - \frac{1}{\tau_{iK}} \right) \rho_{ij} & i \neq K, j = K\end{aligned}\quad (72)$$

for the off-diagonal elements. Equations (69), (71), and (72) can be derived by assuming first-order decay of the diagonal elements, and enforcing conservation of the electronic density and phase angle.<sup>67</sup>

As the system decoheres and demixes, the nuclear momenta are adjusted to conserve total energy

$$\dot{\mathbf{P}}^{\text{DM}} = \dot{\mathbf{P}} + \dot{\mathbf{P}}^{\text{D}}, \quad (73)$$

where it is convenient to write the additional term as

$$\dot{\mathbf{P}}^{\text{D}} = - \sum_{i \neq K} \frac{\dot{V}_i^{\text{D}}}{(\mathbf{P} \cdot \hat{\mathbf{s}}_i)/M} \hat{\mathbf{s}}_i. \quad (74)$$

Equation (74) guarantees that decoherence is turned off as the momentum available in the decoherent direction  $\hat{\mathbf{s}}_i$  goes to zero, with

$$\dot{V}_i^{\text{D}} = \frac{\rho_{ii}}{\tau_{iK}} (V_K - V_i), \quad (75a)$$

$$\dot{V}_i^{\text{D}} = \frac{\rho_{ii}}{\tau_{iK}} W_{KK} - \left( \frac{\rho_{iK}}{\tau_{iK}} + \frac{\rho_{iK}}{\rho_{KK}} \sum_{j \neq K} \frac{\rho_{jj}}{\tau_{jK}} \right) W_{iK} - \frac{1}{2} \left( \frac{1}{\tau_{iK}} + \frac{1}{\tau_{jK}} \right) \rho_{ij} W_{ij}. \quad (75d)$$

The decoherence vector determines the components of  $\mathbf{P}$  into and out of which energy is exchanged as the system decoheres and demixes, and we choose

$$\mathbf{s}_i = (\mathbf{P} \cdot \hat{\mathbf{F}}_{iK} \mathbf{F}_{iK} + \mathbf{P}_{\text{vib}}), \quad (76a)$$

$$\mathbf{s}_i = (\mathbf{P} \cdot \hat{\mathbf{F}}_{iK}^{\text{r}} \mathbf{F}_{iK}^{\text{r}} + \mathbf{P}_{\text{vib}}), \quad (76d)$$

where  $\hat{\cdot}$  denotes a unit vector (as it always does in this whole chapter), and  $\mathbf{P}_{\text{vib}}$  is the vibrational momentum. In regions of strong coupling  $\mathbf{s}_i \approx \mathbf{F}_{iK}$  or  $\mathbf{F}_{iK}^r$ , which is a physically reasonable choice, and when the coupling vanishes (where nonzero  $\mathbf{F}_{iK}$  and  $\mathbf{F}_{iK}^r$  are not defined)  $\mathbf{s}_i \approx \mathbf{P}_{\text{vib}}$ , which is a choice that conserves total angular momentum. The vibrational momentum can be calculated for polyatomics as<sup>99</sup>

$$\mathbf{P}_{\text{vib}}^\alpha = \mathbf{P}^\alpha - M\boldsymbol{\omega} \times \mathbf{Q}^\alpha, \quad (77)$$

where

$$\boldsymbol{\omega} = \mathbf{I}^{-1}\mathbf{J}, \quad (78)$$

$\mathbf{I}$  is the inertial tensor matrix,  $\mathbf{J}$  is the total angular momentum vector,  $\alpha$  labels atoms, and  $\mathbf{P}_{\text{vib}}^\alpha$ ,  $\mathbf{P}^\alpha$ ,  $\boldsymbol{\omega}$ , and  $\mathbf{Q}^\alpha$  are three-dimensional vectors.

A quantum subsystem coupled to an environment does not actually decay to a pure state but rather to a classical, incoherent mixture of states,<sup>100</sup> each associated with a probability of occurring in an ensemble. To incorporate this into the present model, the decoherent state  $K$  is allowed to switch stochastically along a DM trajectory according to a fewest-switches criterion. In the coherent switches (CS) implementation of DM, equations similar to Eqs. (47) and (48) are used to switch  $K$ , with  $\rho_{ij}$  replaced by a locally coherent electronic density matrix  $\rho_{ij}^{\text{CS}}$ . The time evolution of  $\rho_{ij}^{\text{CS}}$  is fully coherent,

$$\dot{\rho}_{ij}^{\text{CS}} = \dot{\rho}_{ij}, \quad (79)$$

i.e. it does not include  $\dot{\rho}_{ij}^{\text{D}}$ , and  $\rho_{ij}^{\text{CS}}$  is made *locally* coherent by setting

$$\rho_{ij}^{\text{CS}} = \rho_{ij}^{\text{DM}} \quad (80)$$

when the trajectory experiences a local minimum in

$$D(t) = \sum_i |\mathbf{F}_{iK}|^2. \quad (81)$$

An ensemble of CSDM trajectories decays to a distribution of final electronic states, and this distribution is determined from the ensemble average,  $\langle \rho_{ii}^{\text{CS}} \rangle$ , obtained from the locally coherent solutions of the classical path equation.

In summary, the CSDM includes the quantum evolution of the electronic degrees of freedom as governed by a reduced density operator (density

matrix), and it incorporates decoherence of the electronic degrees of freedom by the nuclear degrees of freedom. In strong interaction regions it is a mean-field method with the formal and practical advantage (such as representation independence) of the Ehrenfest method, but the decoherence mitigates the disadvantage of the mean-field approach. We note that the CSDM does not scale in a difficult way with system size, and it can easily be applied to large and complex systems.

## 5. Summary of Recent Tests and Applications

The FSTU method (with the SD algorithm and the grad  $V$  prescription for treating the remaining frustrated hops) and the CSDM method are the results of a long series of systematic studies of the NBO dynamics of triatomic and, more recently, polyatomic systems. The FSTU and CSDM methods are straightforward to implement, readily applicable to a wide variety of NBO molecular dynamics simulations with any number of atoms and any number of electronic states, and are available in the distributed computer code ANT.<sup>101</sup> Here we summarize the results of the validation studies that led to the improved methods, and we discuss recent applications. Before doing this we note that large systems may involve new features so there is no guarantee that methods found to be accurate for triatomic and tetraatomic cases are accurate in all cases, including large molecules; however, it is clear that methods that fail even for small molecules are not to be trusted for large molecules and it would be hard to argue that they should ever be preferred. Anyway, as far as test against accurate quantum dynamics for the same sets of potential energy surfaces and couplings, small-molecule tests are all we have at this point in time. Tests comparing NBO molecular dynamics with experimental results are tests against accurate quantum dynamics, but since the exact surfaces and couplings are not known and the extent of possible experimental error is often hard to estimate, such tests are not as straightforward to interpret as small-molecule tests where accurate quantum dynamics are available for given sets of surfaces and couplings.

The FSTU and CSDM NBO molecular dynamics methods, along with several variants and predecessors, were tested against accurate outgoing wave variational principle<sup>41,102–104</sup> quantum mechanical reactive scattering calculations on a series of two-state atom-diatom test cases. Full-dimensional test cases with prototypical AC,<sup>105</sup> WI,<sup>89</sup> and CI<sup>7</sup> interactions

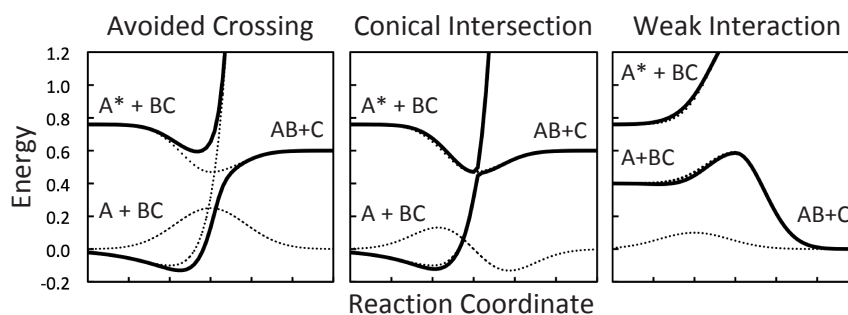
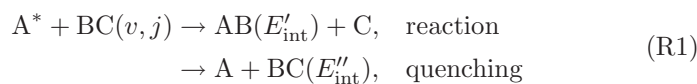


Fig. 1. Examples of the adiabatic (solid) and diabatic (dashed) potential energy surfaces along (left-to-right) the ground state reaction coordinate for the AC, WI, and CI families of test cases.

(as illustrated in reduced dimensionality in Fig. 1) were developed for this purpose, each of which describes a model reaction of the form



where the asterisk denotes electronic excitation, and the diatom is initially prepared in a quantized rovibrational state  $(v, j)$ .

Six observables of the model reactions displayed in R1 were considered: the probability of reactive de-excitation ( $P_R$ ), the probability of nonreactive de-excitation or quenching ( $P_Q$ ), the total probability of a nonadiabatic event ( $P_N = P_R + P_Q$ ), the reactive branching fraction  $F_R = P_R/P_N$ , and the average internal energies of the two diatomic fragments ( $E'_{\text{int}}$  and  $E''_{\text{int}}$ ). Several test cases for each class of prototypical interactions were considered; they vary in the coupling strength of the model potential energy surfaces, the initial conditions, and/or the scattering conditions. By averaging over several test cases in each class, we obtain more robust and predictive error estimates. The results of these studies, which include errors for a total of six observables for each of 17 test cases, are summarized in Table 1.<sup>8</sup>

The 17 test cases in Table 1 include three cases of weak interaction (systems like  $\text{Br}^* + \text{HR} \rightarrow \text{Br} + \text{HR}$  or  $\rightarrow \text{HBr} + \text{R}$ , where R is a radical; these cases are called WI cases or YHR cases), eight cases with accessible regions of avoided crossing but no accessible conical intersections (these are called AC cases or MXH cases), and five cases of accessible conical intersections (these are called CI cases or MCH cases). In each of these 17 cases we obtained accurate quantum dynamics results for a given realistic set of potential energy surfaces and couplings and compared these to

Table 1. Highly-averaged percentage errors for several NBO methods.

Method	Representation	AC	WI	CI	Overall
FS <sup>a</sup>	A	53	29	53	45
	D	42	289	43	125
	CC	53	29	40	41
SE	A/D/CC	74	<sup>c</sup>	66	<sup>c</sup>
FSTU <sup>b</sup>	A	43	25	56	41
	D	27	128	42	66
	CC	38	25	39	34
CSDM	A	20	18	42	27
	D	19	22	33	25
	CC	21	18	33	24

<sup>a</sup>Frustrated hops were ignored.

<sup>b</sup>Frustrated hops were treated using the TU and grad  $V$  prescriptions. The SD algorithm was not used because it had not been developed yet at the time that these calculations were carried out.

<sup>c</sup>The SE method fails for weakly coupled systems in that it does not produce all possible products; therefore average internal energies cannot be computed for the missing products, and an overall error cannot be computed.

the results of various semiclassical dynamics methods for the same potential energy surfaces and couplings and the same initial quantum states. The 17 cases differ from one another in the potential energy surfaces, the couplings, and/or the initial quantum state (for WI cases, there is one set of surfaces, and we ran the ground vibrational-rotational state of the reactants at two energies and one excited rotational state at one energy; for AC cases there are three different couplings surfaces — strong and broadly distributed, strong and localized, and weak and localized, and each was run for three initial rotational states; for CI cases there are five different sets of couplings). The accurate dynamics are independent of representation (adiabatic or diabatic), but the semiclassical results depend on the representation in which the dynamics are calculated; for each case and each representation we calculated the unsigned percentage error in each of the six physical observables mentioned in the previous paragraph by comparing the semiclassical results to the accurate quantum dynamics ones. Each column in the table shows mean unsigned percentage error averaged over the six observables in each of two representations for the cases in that column. The last column contains all 17 cases and so the mean unsigned percentage errors in the last column are averaged over  $6 \times 2 \times 17 = 204$  absolute percentage errors.

The table shows that the results of the NBO molecular dynamics simulations are in general strongly dependent on the choice of electronic representation, and it shows that the adiabatic representation is usually more accurate than the diabatic one. The SE method is formally independent of the choice of representation, but it is less accurate than the other methods. Furthermore, it is unable to treat the small probability events occurring in the WI systems.<sup>8</sup>

The adiabatic representation is not always to be preferred, and the diabatic representation was found to be more accurate for some of the systems in the test set with ACs and CIs. A useful criterion for choosing between the adiabatic and diabatic representations is to prefer the representation where the diagonal surfaces are the least coupled to one another. One way to do this is to prefer the representation with the fewest number of attempted surface hops, and this representation is called the Calaveras County (CC) representation.<sup>106</sup> Results obtained using the CC representation are shown in Table 1. The CC is generally more accurate than using either the adiabatic or diabatic representations exclusively.

For larger systems than the ones considered here, it is likely that trajectories may sample some regions where the adiabatic representation is preferred and others where the diabatic representation is preferred in a single simulation. Invariance to the choice of electronic representation is therefore desirable, and it is encouraging that the CSDM method, which was designed with representation independence as a goal, is systematically less representation-dependent than the FSTU and other NBO molecular dynamics methods.

The overall accuracy of the best representations for each type of improved NBO method is generally good, and the CSDM method is the best method overall with an error of only  $\sim 25\%$ . Clearly the improvements made to the surface hopping approach and to the mean field approach have produced systematically improved methods of each type. Finally, we note that the improved methods work nearly equally well for the three types of interactions considered. Again, this robustness is important, as real systems are likely to feature more than one kind of interaction. Not only does the CSDM provide reasonably accurate final states, but — because of the explicit inclusion of decoherence with a physical time scale — it is expected to provide a realistic picture of the real-time process; the ability of semiclassical methods including decoherence to do this is expected to become more and more useful as shorter time scales<sup>107,108</sup> for studying the electron dynamics in molecules become accessible.

In another test, the accuracy of NBO MD methods for simulating deep quantum systems (i.e. systems with large electronic state energy gaps) was considered.<sup>71</sup> Typical energy gaps in the model AC and WI test cases are only a few tenths of an eV, whereas many real systems have much larger gaps. Quantum mechanical calculations of the photodissociation of the  $\text{Na}\cdots\text{FH}$  van der Waals complex with a gap of  $\sim 1.5$  eV were carried out.<sup>109</sup> In the ground state, thermal excitation tends to break the weak van der Waals bond, producing the Na and HF products exclusively. Upon electronic excitation with visible light, however, the complex is promoted to a metastable complex called an exciplex. The exciplex is proposed to exhibit enhanced reactivity via the harpooning mechanism, where the change in the electronic structure results in a donation of partial charge from the Na atom to the F atom and promotes formation of the  $\text{NaF} + \text{H}$  products.

The FSTU and CSDM methods were shown to fairly accurately predict product branching and exciplex lifetimes for the photodissociation of the  $\text{Na}\cdots\text{FH}$  system, as shown in Table 2, thus validating their use for deep quantum systems. The NBO classical and quantum dynamics simulations confirmed the enhanced reactivity of the harpooning mechanism, and  $\text{NaF} + \text{H}$  was predicted to be the dominant photodissociated bimolecular product.

In the course of this study, product branching in the NBO molecular dynamics simulations was found to be affected by a region of coupling where the excited state is classically energetically forbidden. An analysis of the NBO MD trajectories revealed that the results are sensitive to the treatment of decoherence. Figure 2 shows contour plots of the excited and ground electronic states, as well as hopping information for a subset of trajectories. The initial downward hops occur for a wide range of accessible geometries of the exciplex. More than three-fourths of the trajectories attempted to hop back into the exciplex after their first hop down, but many

Table 2. Product branching probabilities and half lives of the  $\text{Na}\cdots\text{FH}$  exciplex.

Method	$P_{\text{Na+HF}}$	$P_{\text{NaF+H}}$	$t_{1/2}$ , ps
Quantum	0.04	0.96	0.42
FSTU without SD	0.16	0.83	0.85
FSTU with SD	0.05	0.95	0.52
CSDM ( $E_0 = 0.1 E_h$ )	0.29	0.71	0.76
CSDM ( $E_0 = 0.001 E_h$ )	0.06	0.94	0.40

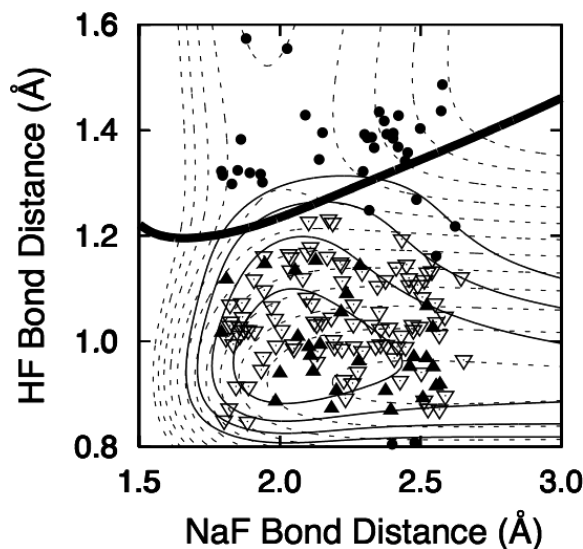


Fig. 2. Contour plots of the ground (dashed) and first excited (solid) potential energy surfaces for  $\text{Na}\cdots\text{FH}$ . The initial hops down are shown as open triangles. Subsequent successful hops up are shown as solid triangles, and frustrated hops up are shown as black dots. The thick black line is the line of avoided crossings.

did so at geometries where the excited state is energetically forbidden. The majority of these frustrated hops occur near the line of avoided crossings, a region where the two electronic surfaces have very different shapes and where decoherence due to wave packet divergence may be expected to be significant. The use of the SD model for decoherence was found to reduce errors associated with frustrated hopping and to predict product branching and lifetimes in near quantitative agreement with the quantum mechanical results, as shown in Table 2. An analogous modification of the DM method resulting in faster decoherence in this critical region (obtained by decreasing the parameter  $E_0$ ) was shown to give similarly improved results. This study highlighted the importance of accurate treatments of electronic decoherence in trajectory-based simulations of systems with coupled electronic states.

In another study,<sup>62</sup> the nonadiabatic photodissociation of HBr was modeled using several NBO trajectory methods. The calculated branching fractions for the  $\text{H} + \text{Br}(^2\text{P}_{3/2})$  and  $\text{H} + \text{Br}(^2\text{P}_{1/2})$  products were found to be in good agreement with experimental measurements<sup>110</sup> over a range of photon energies, as shown in Fig. 3.

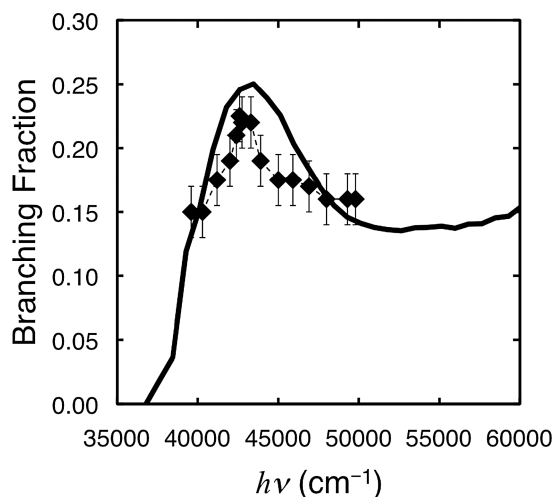


Fig. 3. HBr photodissociation branching fraction to form  $\text{H}+\text{Br}^*$  as a function of photon energy ( $h\nu$ ) obtained by the CSDM method (solid line) and experiment (diamonds).

Li *et al.* applied the CSDM method to several systems: the  $\text{D} + \text{H}_2$  and  $\text{H} + \text{D}_2$  reactions at collision energies up to 2 eV,<sup>111</sup> nonreactive and reactive charge transfer and reactive non-charge-transfer in  $\text{D}^+ + \text{H}_2$  and  $\text{H}^+ + \text{D}_2$  collisions,<sup>111</sup> and intersystem crossing in  $\text{O}(^3\text{P}_{2,1,0}, ^1\text{D}_2) + \text{H}_2$  reactive collisions yielding  $\text{OH}(^2\Pi_{3/2,1/2}) + \text{H}(^2\text{S})$ .<sup>112</sup> For the first two reactions they employed a two-state electronic basis, for the next two a three-state electronic basis, and for the final two a four-state electronic basis (three triplet states and one singlet). For  $\text{D} + \text{H}_2$  and  $\text{H} + \text{D}_2$  they obtained very good agreement of reactive cross sections with accurate quantum dynamics over the whole energy range. For nonreactive and reactive charge transfer in  $\text{D}^+ + \text{H}_2$  and  $\text{H}^+ + \text{D}_2$ , the CSDM cross sections provide overall trends in good agreement with accurate quantum dynamics, and for reactive non-charge-transfer the CSDM cross sections agree with accurate quantum dynamical ones over the whole energy range up to 2.5 eV, although in one case they are slightly lower. For  $\text{O}(^3\text{P}_2) + \text{H}_2$ , the cross sections to produce the  $^2\Pi_{3/2}$  and  $^2\Pi_{1/2}$  states are both in good agreement with accurate quantum dynamics over the whole range of collision energies, up to 28 kcal/mol, except that the cross section to produce the  $^2\Pi_{3/2}$  state has a somewhat higher threshold.

The photodissociation of  $\text{NH}_3$ , which has been studied in detail experimentally,<sup>113,114</sup> was also recently modeled using NBO MD

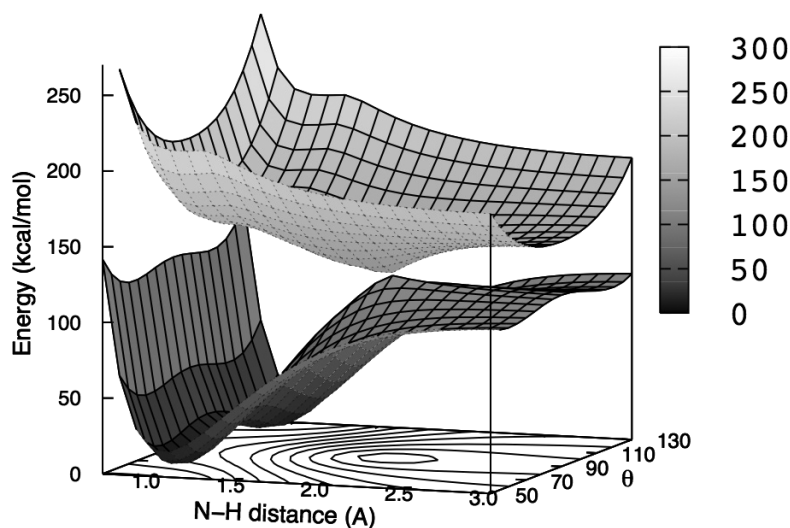


Fig. 4. A conical intersection between the ground and first excited states of NH<sub>3</sub> occurs at planar geometries and at an N-H distance of 2 Å.

simulations.<sup>80,85</sup> Analytic representations<sup>115</sup> of the coupled  $X$  and  $A$  states of NH<sub>3</sub> are shown in Fig. 4 as functions of one N-H distance and the umbrella angle  $\theta$ . This system features a CI at extended N-H distances and planar geometries. Trends in the production of excited state amino radicals as a function of initial state preparation were computed and compared with experiment. The experimental results suggest an enhancement in the production of excited-state products when the antisymmetric stretch of NH<sub>3</sub> is excited, with the interpretation that excitation of the antisymmetric stretch causes the system to go around the CI and thus inhibits electronic state quenching. The NBO MD calculations predict that the production of excited state amino radicals depends on the total energy, and no state specificity is observed. The source of this discrepancy is unclear, although recent quantum mechanical wave packet results<sup>116</sup> are in fair agreement with the NBO trajectory results.

In addition to making semiquantitative predictions of product branching, lifetimes, and internal energy distributions, as discussed above, NBO molecular dynamics simulations are useful for studying chemical events in mechanistic detail, such as the role of conical intersections and avoided crossings in NBO dynamics. This analysis has been carried out

for the FSTU and CSDM methods for the model CI and AC test cases,<sup>7</sup> Na···FH photodissociation,<sup>71</sup> and for the photodissociation of NH<sub>3</sub>.<sup>80,85</sup>

From these studies, one can make some general comments about NBO trajectories and CIs. The capture efficiencies of a CI and an AC have been compared for similar potential energy surfaces, differing only in the interaction type. Trajectories with reasonable kinetic energies were found to be captured equally well by the CI and AC, i.e. the conical shape near the CI did not capture trajectories any more or less easily than an AC. The CI was shown to more efficiently move trajectories out of the interaction region than the AC, although the effect was small. Finally, it was noted that trajectories did not in general switch surfaces at zero-gap geometries. Instead, surface hops occurred over a range of energy gaps, geometries, and coupling strengths near and at the CI.

A similar analysis of the NH<sub>3</sub> trajectories was carried out to study the experimentally proposed mechanism of state specificity. The NBO MD trajectory results showed that the system is efficiently quenched via the seam of CIs when either the antisymmetric or symmetric stretches are excited. The distribution of energy gaps at surface hops was peaked at zero, but the average gap was 0.3 eV. The CI rapidly quenched photoexcited NH<sub>3</sub> nonreactively to form ground-electronic-state NH<sub>3</sub>, which subsequently and much more slowly decayed to NH<sub>2</sub> + H. Only a small fraction of trajectories dissociated directly to the NH<sub>2</sub> + H products. Furthermore, the number of direct trajectories avoiding the CI was not promoted by excitation into the antisymmetric stretch, in contrast to the experimentally proposed mechanism.

## 6. Concluding Remarks

Non-Born–Oppenheimer dynamics may be dominated by regions of conical intersections, by regions of avoided crossings, or by regions of weak interactions of electronic states. When a conical intersection seam or its neighborhood is dynamically accessible, the geometries in the neighborhood of the conical intersections seam will often provide an efficient route for excited state decay, as originally pointed out by Teller.<sup>9</sup> As mentioned in the introduction and as indicated by analyses of non-Born–Oppenheimer trajectories in Sec. 5, the seam of conical intersections — due to its dimensionality being two lower than the dimensionality of the full internal coordinate space — does not necessarily directly mediate electronic transitions; however, the

conical intersection seam does anchor the loci of strong interaction of the potential energy surfaces. Because the conical intersection seam can be a very extended hypersurface, one must consider more than just the lowest-energy conical intersection, and because the conical intersection itself may be dynamically inaccessible, one must consider avoided crossings as well as conical intersections. Because conical intersections are surrounded by avoided crossing regions, it is important to consider the multidimensional character of the dynamics whenever a region of strong interaction of the electronic states is encountered; treatments based on treating the potentials along a trajectory path as one-dimensional avoided crossings ignore the fact that strong interaction regions in polyatomic systems have more complicated dynamics than the Landau–Zener behavior encountered in atom–atom collisions. The best zero-order model of the dynamics in a strong interaction region may be either diabatic or adiabatic. Furthermore, one must take into account the fact that decoherence may occur between successive visits to strong interaction regions. The semiclassical dynamics methods reviewed in this chapter take account of this decoherence; they have been validated in multidimensional studies for the treatment of photochemical dynamics in the vicinity of conical intersections and avoided crossing regions and also in weak interaction regions, they may be used for systems containing both predominantly diabatic and predominantly adiabatic regions of phase space, and rare-event sampling algorithms are available for treating processes with small transition probabilities. The CSDM method, in particular, is the culmination of a series of attempts to improve mean-field and surface hopping methods by combining the best features of both.

### Acknowledgments

This work was supported in part by the National Science Foundation and in part by the Division of Chemical Sciences, Geosciences, and Biosciences, Office of Basic Energy Sciences, U.S. Department of Energy under Contract No. DE-AC04-94-AL85000.

### References

1. J.C. Tully, in *Modern Methods for Multidimensional Dynamics Computations in Chemistry*, edited by D.L. Thompson (World Scientific, Singapore, 1998), pp. 34–72.

2. E.E. Nikitin, *Annu. Rev. Phys. Chem.* **50**, 1 (1999).
3. A.W. Jasper, B.K. Kendrick, C.A. Mead and D.G. Truhlar, in *Modern Trends in Chemical Reaction Dynamics: Experiment and Theory, Part I*, edited by X. Yang and K. Liu (World Scientific, Singapore, 2004), pp. 329–391. [*Adv. Ser. Phys. Chem.* **14**, 329 (2004)].
4. G.A. Worth and L.S. Cederbaum, *Annu. Rev. Phys. Chem.* **55**, 127 (2004).
5. A.W. Jasper, S. Nangia, C. Zhu and D.G. Truhlar, *Acc. Chem. Res.* **39**, 101 (2006).
6. J.M. Bowman, *Science* **319**, 40 (2008).
7. A.W. Jasper and D.G. Truhlar, *J. Chem. Phys.* **122**, 044101 (2005).
8. A.W. Jasper, C. Zhu, S. Nangia and D.G. Truhlar, *Faraday Discuss. Chem. Soc.* **127**, 1 (2004).
9. E. Teller, *J. Phys. Chem.* **41**, 109 (1937).
10. K.A. Kistler and S. Matsika, *J. Chem. Phys.* **128**, 215102 (2008).
11. G.J. Atchity, S.S. Xantheas and K. Ruedenberg, *J. Chem. Phys.* **95**, 1862 (1991). D.R. Yarkony, *J. Phys. Chem. A* **105**, 985 (1996).
12. V. Bonacic-Koutecky, J. Koutecky and J. Michl, *Angew. Chem. Int. Ed.* **26**, 170 (1987).
13. M. Olivucci, I.N. Ragazos, F. Bernardi and M.A. Robb, *J. Am. Chem. Soc.* **115**, 371 (1993).
14. L. Seidner and W. Domcke, *Chem. Phys.* **186**, 27 (1994).
15. W. Fu, S. Lochbrunner, A.M. Müller, T. Schikarski, W.E. Schmid and S.A. Trushin, *Chem. Phys.* **232**, 16 (1998).
16. L. Serrano-Andrés, M. Merchán and A.C. Borin, *Proc. Nat. Acad. Sci. U. S. A.* **103**, 8691 (2004).
17. J. Michl, *Mol. Photochem.* **4**, 243 (1972).
18. H.E. Zimmerman, *Acc. Chem. Res.* **15**, 312 (1982).
19. E. Teller, *Israel J. Chem.* **7**, 227 (1969).
20. D.G. Truhlar and C.A. Mead, *Phys. Rev. A* **68**, 032501 (2003).
21. D.G. Truhlar, *Faraday Discuss. Chem. Soc.* **127**, 242 (2004).
22. T.C. Allison, G.C. Lynch, D.G. Truhlar and M.S. Gordon, *J. Phys. Chem.* **100**, 13575 (1996).
23. O. Tishchenko, D.G. Truhlar, A. Ceulemans and M.T. Nguyen, *J. Am. Chem. Soc.* **130**, 7000 (2008).
24. A.W. Jasper, S.N. Stechmann and D.G. Truhlar, *J. Chem. Phys.* **116**, 5424 (2002); **117**, 10427(E) (2002).
25. A. Bjerre and E.E. Nikitin, *Chem. Phys. Lett.* **1**, 179 (1967).
26. R.K. Preston and J.C. Tully, *J. Chem. Phys.* **54**, 4297 (1971).
27. N.C. Blais and D.G. Truhlar, *J. Chem. Phys.* **79**, 1334 (1983).
28. C. Zhu, S. Nangia, A.W. Jasper and D.G. Truhlar, *J. Chem. Phys.* **121**, 7658 (2004).
29. H.-D. Meyer and W.H. Miller, *J. Chem. Phys.* **70**, 3214 (1979).
30. A.D. Micha, *J. Chem. Phys.* **78**, 7138 (1983).
31. M. Amarouche, F.X. Gadea and J. Durup, *Chem. Phys.* **130**, 145 (1989).
32. A. Donoso and C.C. Martens, *Int. J. Quantum Chem.* **90**, 1348 (2002).

33. R. Kapral and G. Ciccotti, *J. Chem. Phys.* **110**, 8919 (1999).
34. M. Santer, U. Manthe and G. Stock, *J. Chem. Phys.* **114**, 2001 (2001).
35. H. Nakamura, *J. Phys. Chem. A* **110**, 10929 (2006).
36. T.J. Martinez, M. Ben-Nun and R.D. Levine, *J. Phys. Chem.* **100**, 7884 (1996).
37. M.D. Hack, A.M. Wensmann, D.G. Truhlar, M. Ben-Nun and T.J. Martinez, *J. Chem. Phys.* **115**, 1172 (2001).
38. M. Ben-Nun and T.J. Martinez, *Adv. Chem. Phys.* **121**, 439 (2002).
39. T.J. Martinez, *Acc. Chem. Res.* **39**, 119 (2006).
40. S. Yang, J.D. Coe, B. Kaduk and T.J. Martínez, *J. Chem. Phys.* **130**, 134113 (2009).
41. G.J. Tawa, S.L. Mielke, D.G. Truhlar and D.W. Schwenke, in *Advances in Molecular Vibrations and Collisional Dynamics*, edited by J.M. Bowman, (JAI, Greenwich, CT, 1994). pp. 45–116.
42. M.D. Hack, A.W. Jasper, Y.L. Volobuev, D.W. Schwenke and D.G. Truhlar, *J. Phys. Chem. A* **103**, 6309 (1999).
43. U. Manthe, H.-D. Meyer and L.S. Cederbaum, *J. Chem. Phys.* **97**, 3199 (1992).
44. H.-D. Meyer and G.A. Worth, *Theor. Chem. Acc.* **109**, 251 (2003).
45. S. Woittequand, C. Toubin, M. Monnerville, S. Briquez, B. Pouilly and H.-D. Meyer, *J. Chem. Phys.* **131**, 194303 (2009).
46. J.O. Hirschfelder and W.J. Meath, *Adv. Chem. Phys.* **12**, 3 (1967).
47. W. Kolos and L. Wolniewicz, *J. Chem. Phys.* **41**, 3663 (1964).
48. B.C. Garrett and D.G. Truhlar, *J. Chem. Phys.* **82**, 4543 (1985).
49. N.F. Zokov, O.L. Polyansky, C.R. LeSueur and J. Tennyson, *Chem. Phys. Lett.* **260**, 381 (1996).
50. D.W. Schwenke, *J. Phys. Chem. A* **105**, 2352 (2001).
51. T.F. O'Malley, *Adv. At. Mol. Phys.* **7**, 223 (1971).
52. H. Köppel, in *Conical Intersections: Electronic Structure, Dynamics and Spectroscopy*, edited by W. Domcke, D.R. Yarkony and H. Köppel (World Scientific, Singapore, 2004), pp. 175–204. [*Adv. Ser. Phys. Chem.* **15**, 175 (2004)].
53. C.A. Mead and D.G. Truhlar, *J. Chem. Phys.* **77**, 6090 (1982).
54. R. Abrol and A. Kuppermann, *J. Chem. Phys.* **116**, 1035 (2002).
55. B.N. Papas, M.S. Schuurman and D.R. Yarkony, *J. Chem. Phys.* **129**, 124104 (2008).
56. V.M. Garcia, M. Reguero, R. Caballol and J.P. Malrieu, *Chem. Phys. Lett.* **281**, 161 (1987).
57. G.J. Atchity and K. Ruedenberg, *Theor. Chem. Acc.* **97**, 47 (1997).
58. H. Nakamura and D.G. Truhlar, *J. Chem. Phys.* **115**, 10353 (2001).
59. H. Nakamura and D.G. Truhlar, *J. Chem. Phys.* **117**, 5576 (2002).
60. H. Nakamura and D.G. Truhlar, *J. Chem. Phys.* **118**, 6816 (2003).
61. R. Valero and D.G. Truhlar, *J. Phys. Chem. A* **111**, 8536 (2007).
62. R. Valero, D.G. Truhlar and A.W. Jasper, *J. Phys. Chem. A* **112**, 5756 (2008).
63. J.C. Tully, *J. Chem. Phys.* **93**, 1061 (1990).

64. V. May and O. Kühn, *Charge and Energy Transfer Dynamics in Molecular Systems* (Wiley-VCH, Berlin, 2000).
65. C. Zhu, A.W. Jasper and D.G. Truhlar, *J. Chem. Theory Comput.* **1**, 527 (2005).
66. D.G. Truhlar, in *Quantum Dynamics of Complex Molecular Systems*, edited by D.A. Micha and I. Burghardt (Springer, Berlin, 2007), pp. 227–243.
67. M.D. Hack and D.G. Truhlar, *J. Chem. Phys.* **114**, 9305 (2001).
68. B.J. Schwartz, E.R. Bittner, O.V. Prezhdo and P.J. Rossky, *J. Chem. Phys.* **104**, 5942 (1996).
69. O.V. Prezhdo and P.J. Rossky, *J. Chem. Phys.* **107**, 5863 (1997).
70. G. Granucci and M. Persico, *J. Chem. Phys.* **126**, 134114 (2007).
71. A.W. Jasper and D.G. Truhlar, *J. Chem. Phys.* **127**, 194306 (2007).
72. D.L. Bunker, *Methods Comp. Phys.* **10**, 287 (1971).
73. M. Karplus, R.N. Porter and R.D. Sharma, *J. Chem. Phys.* **43**, 3259 (1965).
74. D.G. Truhlar and J.T. Muckerman, in *Atom-Molecule Collision Theory: A Guide for the Experimentalist*, edited by R.D. Bernstein (Plenum, New York, 1979), pp. 505–566.
75. L.M. Raff and D.L. Thompson, in *Theory of Chemical Reaction Dynamics, Vol. 3*, edited by M. Baer (CRC Press, Boca Raton, 1985), pp. 1–121.
76. J.J. Sakurai, *Modern Quantum Mechanics* (Addison-Wesley, Reading, 1985), pp. 335–339.
77. R. Schinke, *Photodissociation Dynamics* (Cambridge University Press, Cambridge, 1993).
78. G. Herzberg, *Molecular Spectra and Molecular Structure. III. Electronic Spectra and Electronic Structure of Polyatomic Molecules* (van Nostrand Reinhold, Princeton, New York, 1966), pp. 149.
79. L. Pauling and E.B. Wilson, *Introduction to Quantum Mechanics: With Applications to Chemistry* (McGraw-Hill, New York, 1935), pp. 73–77.
80. D. Bonhommeau and D.G. Truhlar, *J. Chem. Phys.* **129**, 014302 (2008).
81. H.-W. Lee and M.O. Scully, *J. Chem. Phys.* **73**, 2238 (1980).
82. J.C. Gray and D.G. Truhlar, *J. Chem. Phys.* **76**, 5350 (1982).
83. E.J. Heller and R.C. Brown, *J. Chem. Phys.* **75**, 1048 (1981).
84. S. Chapman, *Adv. Chem. Phys.* **82**, 423 (1992).
85. A.W. Jasper and D.G. Truhlar, *Chem. Phys. Lett.* **369**, 60 (2003).
86. D. Bomhommeau, R. Valero, D.G. Truhlar and A.W. Jasper, *J. Chem. Phys.* **130**, 234303 (2009).
87. M.F. Herman, *J. Chem. Phys.* **81**, 754 (1984).
88. J.-Y. Fang and S. Hammes-Schiffer, *J. Chem. Phys.* **110**, 11166 (1999).
89. A.W. Jasper, M.D. Hack and D.G. Truhlar, *J. Chem. Phys.* **115**, 1804 (2001).
90. U. Müller and G. Stock, *J. Chem. Phys.* **107**, 6230 (1997).
91. M. Thachuk, M.Y. Ivanov and D.M. Wardlaw, *J. Chem. Phys.* **109**, 5747 (1998).
92. J.-Y. Fang and S. Hammes-Schiffer, *J. Phys. Chem. A* **103**, 9399 (1999).
93. A.W. Jasper and D.G. Truhlar, *J. Chem. Phys.* **123**, 064103 (2005).

94. S. Nangia, A.W. Jasper, T.F. Miller III and D.G. Truhlar, *J. Chem. Phys.* **120**, 3586 (2004).
95. R.T. Skodje and D.G. Truhlar, *J. Chem. Phys.* **80**, 3123 (1984).
96. G.A. Worth, M.A. Robb and B. Lasorne, *Mol. Phys.* **106**, 2077 (2008).
97. C. Zhu, A.W. Jasper and D.G. Truhlar, *J. Chem. Phys.* **120**, 5543 (2004).
98. S.C. Cheng, C. Zhu, K.K. Liang, S.H. Lin and D.G. Truhlar, *J. Chem. Phys.* **129**, 024112 (2008).
99. W.L. Hase, D.G. Buckowski and K.N. Swamy, *J. Phys. Chem.* **87**, 2754 (1983).
100. A. Bohm, *Quantum Mechanics: Foundations and Applications*, 3rd ed. (Springer-Verlag, New York, 1983), pp. 57–73.
101. Z.H. Li, A.W. Jasper, D.A. Bonhommeau, R. Valero and D.G. Truhlar, ANT-version 2009 (University of Minnesota, Minneapolis, 2009).
102. Y. Sun, D.J. Kouri, D.G. Truhlar and D.W. Schwenke, *Phys. Rev. A* **41**, 4857 (1990).
103. D.W. Schwenke, S.L. Mielke, G.J. Tawa, R.S. Friedman, P. Halvick and D.G. Truhlar, *Chem. Phys. Lett.* **203**, 565 (1973).
104. G.J. Tawa, S.L. Mielke, D.G. Truhlar and D.W. Schwenke, *J. Chem. Phys.* **100**, 5751 (1994).
105. Y.L. Volobuev, M.D. Hack, M.S. Topaler and D.G. Truhlar, *J. Chem. Phys.* **112**, 9716 (2002).
106. M.D. Hack and D.G. Truhlar, *J. Phys. Chem. A* **104**, 7917 (2000).
107. M. Wickenhauser, J. Burgdörfer, F. Krausz and M. Drescher, *Phys. Rev. Lett.* **94**, 023002 (2005).
108. F. Krausz and M. Ivanov, *Rev. Mod. Phys.* **81**, 163 (2009).
109. S. Garashchuk and V.A. Rassolov, *Chem. Phys. Lett.* **446**, 395 (2007).
110. P.M. Regan, S.R. Langford, A.J. Orr-Ewing and M.N.R. Ashfold, *J. Chem. Phys.* **110**, 281 (1999).
111. B. Li, T.-S. Chu and K.-L. Han, *J. Comput. Chem.* **31**, 362 (2010).
112. B. Li and K.-L. Han, *J. Phys. Chem. A* **113**, 10189 (2009).
113. A. Bach, J.M. Hutchison, R.J. Holiday and F.F. Crim, *J. Phys. Chem. A* **107**, 10490 (2003).
114. M.L. Hause, Y.H. Yoon and F.F. Crim, *J. Chem. Phys.* **125**, 174309 (2006).
115. Z.H. Li, R. Valero and D.G. Truhlar, *Theor. Chem. Acc.* **118**, 9 (2007).
116. W. Lai, S.Y. Lin, D. Xie and H. Guo, *J. Phys. Chem. A* **114**, 3121 (2010).